Solar Energy 233 (2022) 363–377

Contents lists available at ScienceDirect

Solar Energy

journal homepage: www.elsevier.com/locate/solener

Plasmonic gold nanoparticle incorporated MgO-coated SnO_2 photoanode for efficiency enhancement in dye-sensitized solar cells

M.A.K.L. Dissanayake [a,b,*], K. Umair [a,b], G.K.R. Senadeera [a,c], T. Jaseetharan [d], A.M.J.S. Weerasinghe [e], H.W.M.A.C. Wijayasinghe [a]

[a] National Institute of Fundamental Studies, Kandy, Sri Lanka
[b] Postgraduate Institute of Science, University of Peradeniya, Peradeniya, Sri Lanka
[c] Department of Physics, The Open University of Sri Lanka, Nawala, Nugegoda, Sri Lanka
[d] Department of Physical Sciences, South Eastern University of Sri Lanka, Sammanthurai, Sri Lanka
[e] School of Chemistry and Physics, Queensland University of Technology, Brisbane 4000, Queensland, Australia

ARTICLE INFO

Keywords:
Dye solar cells
SnO_2@MgO photoanode
Gold nanoparticles
LSPR effect
Charge recombination

ABSTRACT

SnO_2 is an attractive semiconducting material suitable for application as the photoanode in dye sensitized solar cells (DSSCs) due to its wide energy band gap and notable photo stability. However, improved solar cell performance can be achieved only by using composites of SnO_2 with other materials like MgO, ZnO, Al_2O_3 and $CaCO_3$. In this study, plasmonic DSSCs were fabricated using MgO coated SnO_2 (SnO_2:MgO) based photoanodes incorporating gold nanoparticles (Au NP) having the size in the 30 – 35 nm range and sensitized with ruthernium N719 dye. Photoanodes were characterized by UV–VIS spectroscopy and the DSSCs were characterized by current–voltage (*J–V)* measurements, incident photon-to-electron conversion efficiency (IPCE) measurements and electrochemical impedance spectroscopy (EIS). Under the illumination of 100 mW cm^{-2} (AM 1.5), the efficiency (η) of the reference DSSC with pristine SnO_2 photoanode was 1.52%, where as the efficiency of the optimized plasmonic DSSC with Au NP incorporated SnO_2:MgO photoanode (Au: SnO_2:MgO) was an impressive 4.69%. This efficiency enhancement of about 208% compared to the reference DSSC appears to be due to the increased open-circuit voltage (V_{OC}) of 725.6 and increased short-circuit photocurrent density (J_{SC}) of 9.06 mA cm^{-2} respectively evidently caused by the reduced electron recombination by ultra-thin MgO barrier layer and the enhanced light harvesting caused by the local surface plasmon resonance (LSPR) effect due to Au nanopraticles. EIS analysis showed that the incorporation of plasmonic Au metal nanoparticles leads to a decrease in the series resistance (R_S) and the interfacial charge-transfer resistance (R_{CT}) at the SnO_2/electrolyte interface.

1. Introduction

Tin oxide (SnO_2) is a promising and reliable candidate to be used as a photoanode in dye-sensitized solar cells (DSSCs) due to its low cost, abundance, wide energy band gap (~3.62 eV at 300 K), high stability and high electron mobility compared to TiO2 (Birkel et al., 2012; O'Regan and Grätzel, 1991; Gong et al., 2017). However, the high back-electron transfer rate of SnO_2 is related to its low value of conduction band edge which accelerates the recombination of electrons and impedes the electron trapping density. The efficiencies reported for SnO_2-based DSSCs have been rather low due to the high rate of recombination of the photo-generated electrons with the oxidized dye or I_3^- ions in the electrolyte (Snaith and Ducati, 2010; Baraneedharan et al., 2014). In order to reduce the recombination losses, utilization of a coated configuration has been introduced (Baraneedharan et al., 2014; Bhande et al., 2014; Zainudin et al., 2019; Wali et al., 2016; Tennakone et al., 2001; Senadeera et al., 2018) The idea is to coat the exposed surface of the SnO_2 semiconductor nanoparticle network with a wide band gap semiconductor such as ZnO, ZrO_2 or an insulator such as MgO, Al_2O_3 and $CaCO_3$ etc. According to Tennakone *et al,* a thin layer of the MgO insulator material in the order of 1 nm coated around the semiconductor particles significantly suppresses the quenching of the photo-generated electrons by recombining with the oxidized dye molecules or the acceptors in the electrolyte (Tennakone et al., 2001). Since the excited level of the dye (D*) is located well above the conduction band of SnO_2 (Fig. 1(b)), it becomes energetically feasible for the photoexcited

* Corresponding author at: National Institute of Fundamental Studies, Kandy, Sri Lanka.
E-mail address: lakshman.di@nifs.ac.lk (M.A.K.L. Dissanayake).

https://doi.org/10.1016/j.solener.2022.01.038
Received 24 July 2021; Received in revised form 1 January 2022; Accepted 17 January 2022

electron of the dye in the outer MgO thin layer of SnO_2 surface to directly tunnel into the conduction band (CB) of SnO_2 easily (Tennakone et al., 2001; Sato, 1998). As shown in Fig. 1(b), when electrons tunnel into SnO_2 (Green colour, dotted line) and relax at the CB, the reverse tunneling probability is largely reduced (Red colour, dash lines). Thus, the MgO barrier suppresses recombination of the electrons with the dye (D) or the electrolyte. The equation below shows that the open-circuit voltage, $V_{OC,}$ depends on the saturation current of the solar cell and the photo-generated current (I_{SC}). While I_{SC} typically has a small variation, the key effect is the saturation current, I_0 since this may vary by orders of magnitude. The saturation current, I_0 depends on recombination in the solar cell. Open-circuit voltage is then a measure of the amount of recombination in the device. According to the following equations, the V_{OC} and the J_{SC} will increase with reduction of recombination (Augusto et al., 2017).

$$V_{oc} = \frac{nk_BT}{e} In\left(\frac{I_{SC}}{I_0}+1\right)$$

$$V_{OC} = \frac{kT}{q}\ln\left(\frac{(N_A+\Delta p)\Delta n}{n_i^2}+1\right)$$

where, kT/q is the thermal voltage, N_A is the doping concentration, Δn is the excess carrier concentration and n_i is the intrinsic carrier concentration (Sinton and Cuevas, 1996).

Further, there are few other interesting phenomena that have been used to enhance the performance of dye-sensitized solar cells. In particular, the effect of local surface plasmon resonance (LSPR) effect arising from noble metal nanoparticles, such as gold (Au NP) and silver (Ag NP) have been used to increase the optical absorption and hence the photocurrent in plasmonic DSSCs (Meen et al., 2013; Chandrasekharan and Kamat, 2000; Dissanayake et al., 2020; Aponsu et al., 2010; Dissanayake et al., 2016). Au NPs have been extensively used for this purpose due their unique optical absorption properties. At a specific wavelength of the incident light, which is a characteristic of the type of the metal, collective oscillations of electrons on the nanoparticle surface cause the Local Surface Plasmon Resonance (LSPR) resulting in strong extinction of light (absorption and scattering). The particular wavelength, or frequency, of light where this occurs is strongly dependent on the metal type, nanoparticle size, shape, surface, and agglomeration state. The LSPR effect increases and strengthens the electromagnetic fields near the metal NPs, leading to the precise control of optical fields and the enhanced absorption band in the UV–VIS spectrum. The use of the plasmonic effect for light trapping provides an efficient way to make the optimum use of the dyes for enhancing solar cell efficiency (Notarianni et al., 2014; Mandal and Sharma, 2016).

The main idea of the present work is the incorporation of plasmonic gold nanoparticles in to the MgO-coated SnO_2 photoanode based DSSCs and evaluate their enhanced photovoltaic performance. Optimization and detailed characterization were done on the effect of variation of film thickness, amount of MgO (ww%) and the volume effect of Au NPs on the photovoltaic performance of the DSSCs. To our knowledge there is no report on the plasmonic effect in MgO-coated SnO_2 photoanode structure for DSSCs.

2. Experimental

2.1. Preparation of gold nanoparticle colloidal suspensions

Gold nanoparticles (AuNPs) were synthesized by using the citrate reduction method. In this method, tetrachloroauric acid (~49% $HAuCl_4$. aq, Fluka) and trisodium citrate dihydrate ($Na_3C_6H_5O_7{\cdot}2H_2O$, Sigma-Aldrich) were used as starting materials. A 20 ml solution of 1.0 mM of $HAuCl_4$ was prepared by adding deionized water to 1% $Na_3C_6H_5O_7$ solution prepared by dissolving 0.1 g of the salt in 10 ml of distilled water. 2 0.0 ml of the trisodium citrate solution was added drop by drop to the boiling solution of 1 mM $HAuCl_4$ under continuous stirring. The color of the solution mixture gradually changed from dark blue to wine red. After the colour change was observed as wine red, the gold particle colloidal solution was kept on mixing and allowed to cool down (Dissanayake et al., 2016; Amir Tabrizi et al., 2009; Huang and Yang, 2003).

2.2. Optical absorption measurements

Optical absorption spectra of the Au NP solution was taken by using

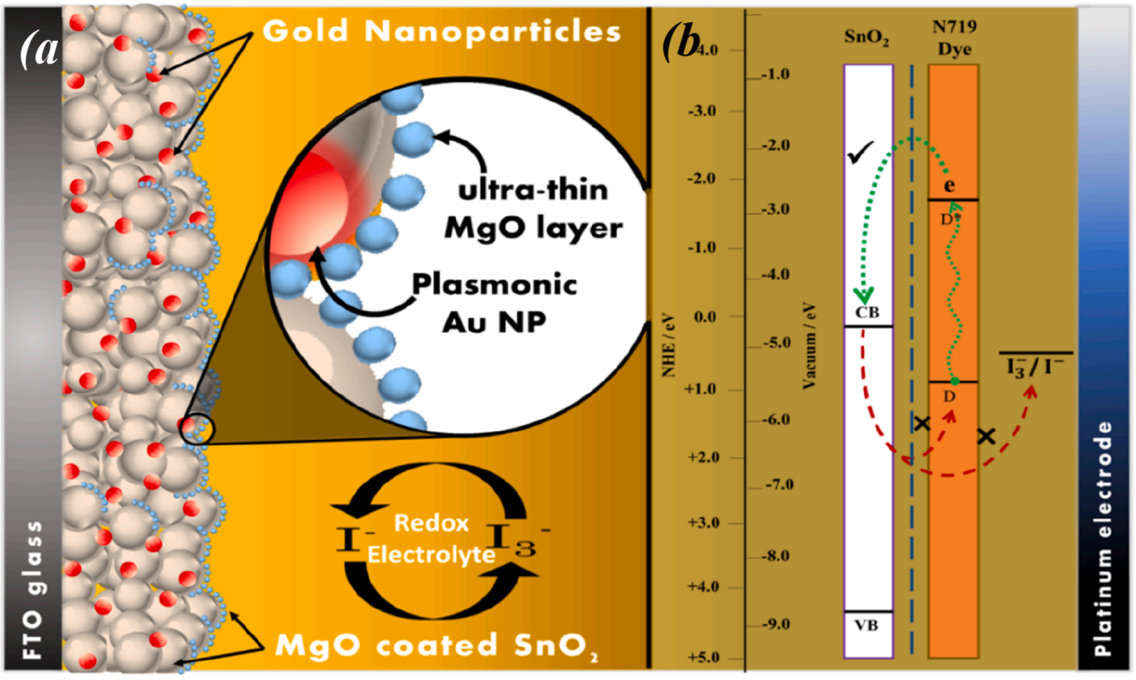

Fig. 1. (a) Graphical image of MgO-coated SnO_2 photoanode and (b) the schematic energy level diagram indicating the position (eV) of the bands of SnO_2 and MgO, ground & excited levels of the N719 dye (D & D*), the I_3^-/I^- redox potential level and work function of gold.

the Shimadzu 2450 UV–VIS spectrophotometer in the wavelength range from 200 nm to 1200 nm.

2.3. Preparation of SnO_2 based photoanodes

Preparation of bare SnO_2 films was done as follows. 2.0 ml of SnO_2 colloidal solution (Alfa chemicals, 15 % SnO_2 colloidal in H_2O) was grounded together with 3 drops of glacial acetic acid and 3 drops of Triton-X 100 using an agate mortar. The mixture was dispersed in 40 ml of ethanol and ultrasonicated for 10–15 min. The sonicated dispersion was sprayed on to 1.0 × 2.0 cm^2 area of cleaned fluorine doped tin oxide (FTO) glass plates (7 Ω/sq sheet from Solaronix) and kept on a hot plate maintained at 150 °C and then sintered at 550 °C in a furnace for 45 min. (A spraying experimental setup is shown Fig. 2).

When the spray solution SnO_2 or SnO_2 + MgO or SnO_2 + MgO + AuNP in ethanol is deposited on the heated substrate the solvent evaporates by leaving the respective solid powder films (SnO_2 or SnO_2 + MgO or SnO_2 + MgO + AuNP) on top of the FTO glass plates (Fig. 3). After sintering at 550 °C for 45 min, no new phases were formed according to the XRD analysis.

The method used to prepare the MgO coated SnO_2 phtoanode is similar to the method reported by Tennakone et al. SnO_2:MgO photoanode were prepared by using 2.0 ml of SnO_2 colloidal suspension, different amounts (3.8, 4.6, 5.1, 8.0,10.0, and 12 ww%) of anhydrous MgO nanoparticles and 3 drops of glacial acetic acid were mixed together in an agate mortar and grounded well with 3 drops of Triton X-100. The mixture was dispersed in 40 ml of ethanol and then sonicated and sprayed on FTO substrates and finally sintered as in the case of bare SnO_2.The presence of MgO coating is confirmed by the Tennakone el al (Tennakone et al., 2001).

Gold nanoparticle incorporated SnO_2:MgO composite photoanodes (AuNP:SnO_2:MgO) were fabricated as follows. A known volume (0.1 ml, 0.2 ml, 0.3 ml, 0.35 ml and 0.4 ml) of Au NP solution was added in to the above weight percentage optimized SnO_2:MgO composite and the mixture was then dispersed in a 40 ml absolute ethanol and ultra sonicated for 10–15 min. Then sonicated mixture was sprayed and sintered as same as above. Subsequently, all the SnO_2 based films (bare SnO_2, SnO_2:MgO and AuNP:SnO_2:MgO) were dipped in the ethanolic dye (0.3 mM) solution containing Ruthenizer 535-bisTBA, [N719, *cis*-diisothiocyanato-bis(2,2′-bipyridyl-4,4′-dicarboxylic acid) ruthenium(II)] dye for 24 h. The four stages of the photoanodes prepared are shown in Fig. 4. The thickness of the photoanodes was varied by spraying different volumes of the precursor solution on different substrates for a known time.

2.4. Solar cell fabrication and I-V characterization

The electrolyte for the DSSCs was prepared by dissolving tetrapropyl ammonium iodide (TPA^+I^-) salt and iodine, I_2 in molten ethylene carbonate and acetonitrile (Kumari et al., 2017). DSSCs were fabricated by sandwiching the above electrolyte solution in the configuration of FTO/ Photoanode/dye/ electrolyte/Pt where the photoanode was one of the

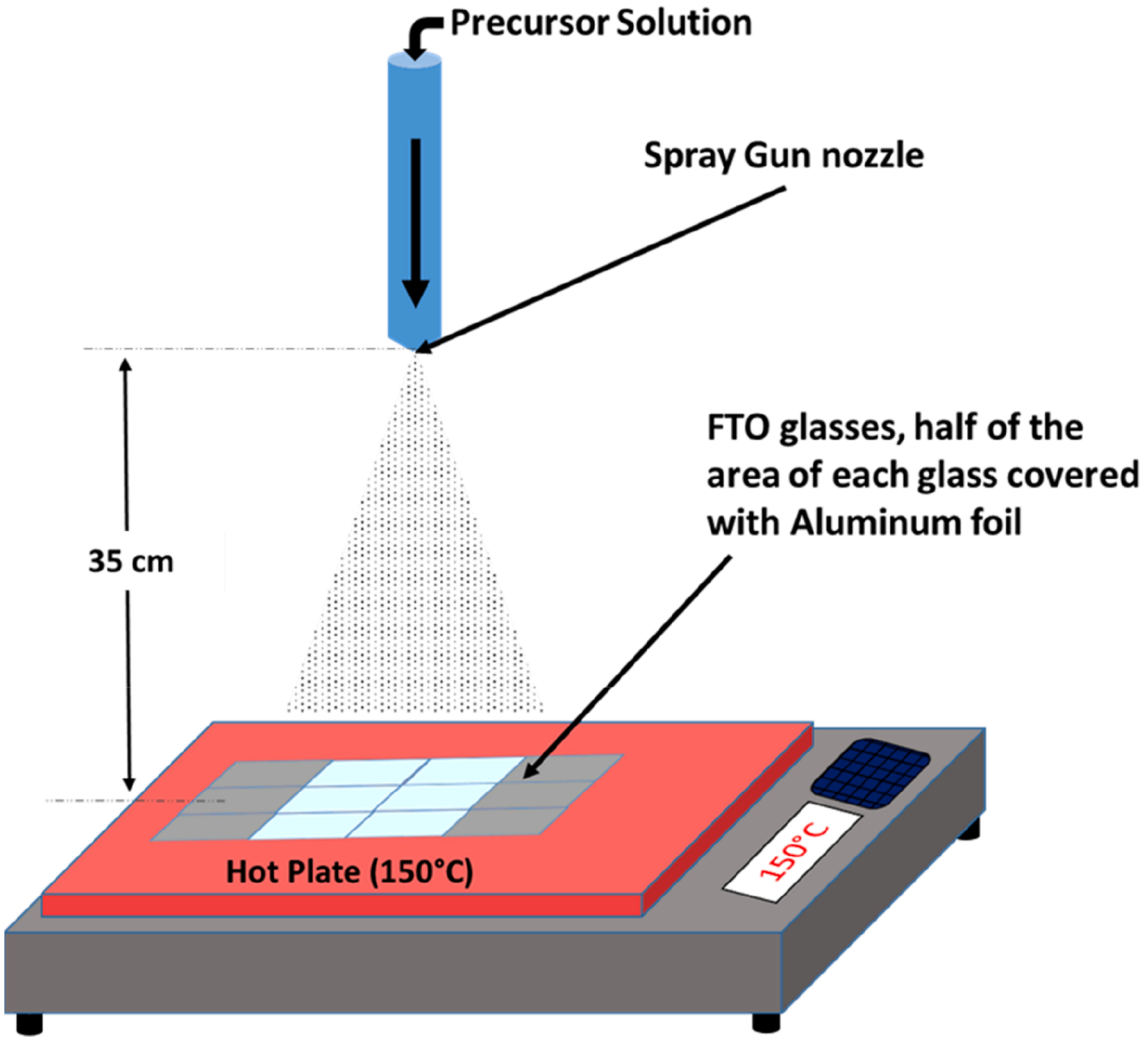

Fig. 2. Schematic diagram of the spray experimental set up.

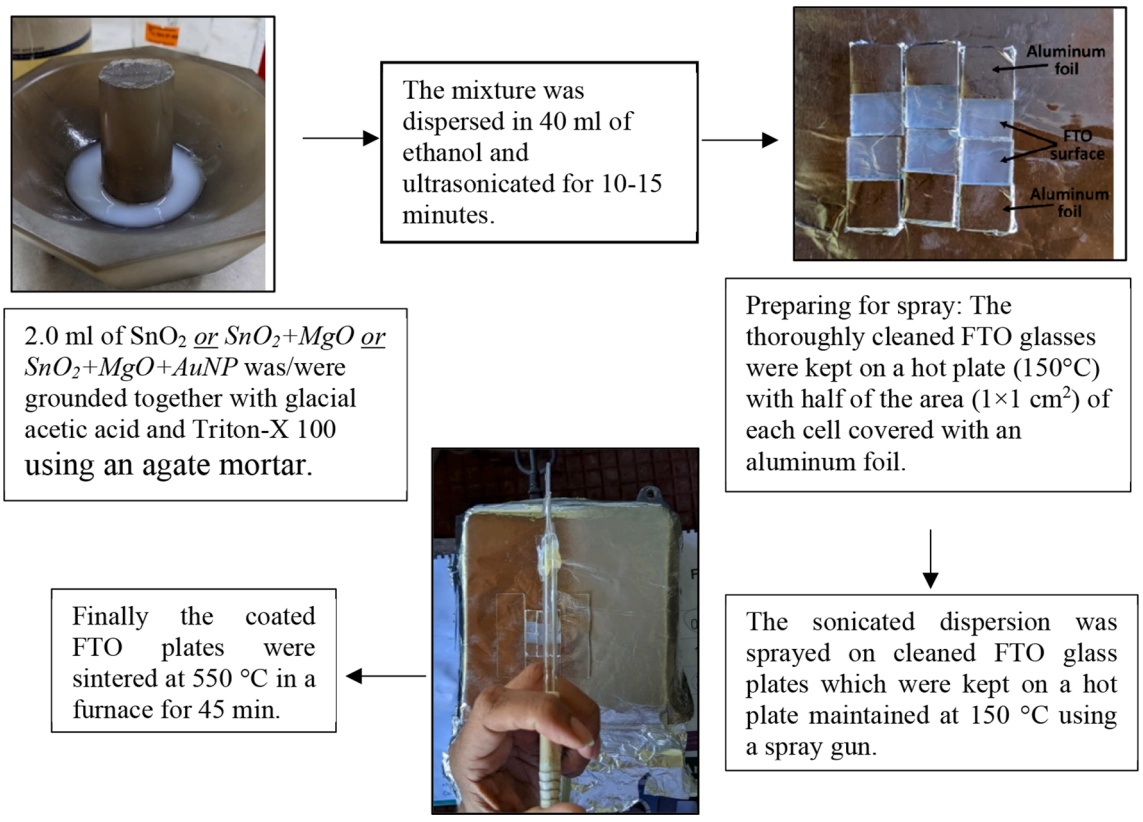

Fig. 3. Steps of spray assisted photoanode preparation.

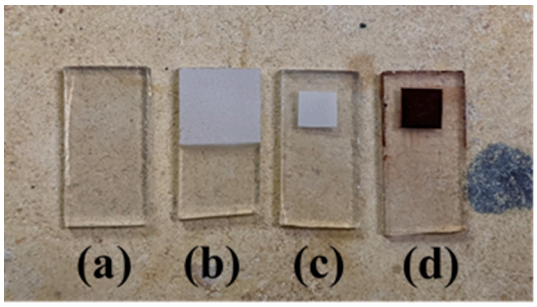

Fig. 4. Four stages of photoanode: (a) Cleaned FTO glass plate (b) Sintered SnO_2:MgO cell (c) Photoanode before Dye dipping (Cell area – 0.25 cm^2) (d) Photoanode after Dye adsorption.

three types (a)SnO_2 or (b) SnO_2:MgO or (c) Au: SnO_2:MgO. The photocurrent density versus voltage measurements were taken for these DSSCs under the illumination of 100 mW cm^{-2} (1.5 AM filter) simulated sunlight with a 100 W Ozone Free Xenon Lamp and a Oriel LCS-100 solar simulator using a Metrohm Autolab Potentiostat/Galvanostat PGSTAT 128. The active area of each cell was 0.25 cm^2.

2.5. Flat-band potential measurements

Flat band potential of a photoanode can be used to understand the movement of the Fermi Level of the MgO insulator layer incorporated SnO_2 electrode and the Au NP incorporated SnO_2:MgO photoanode with respect to the reference photoanode. In order to find the flat band potential of the three SnO_2 based electrodes, Mott-Schottky measurements were taken by immersing each of the three electrodes, (a) bare SnO_2, (b) SnO_2:MgO and (c) Au: SnO_2:MgO in a 0.5 M Na_2SO_4 electrolyte solution, one at a time. The stabilized voltage was measured with respect to a standard calomel electrode (SCE) using a Metrohm Autolab PGSTAT 128 N potentiostat. The scanned frequencies were 1000 Hz and 1500 Hz.

2.6. XRD measurements

Crystalline phase of the samples (bare SnO_2, SnO_2:MgO and AuNP: SnO_2:MgO) were characterized using an X-ray diffractometer radiation over the range of 2θ angles from 20° to 70°.

2.7. IPCE and optical absorption measurements

The Incident Photon-to-electron Conversion Efficiency (IPCE) is the conversion ratio of the incident photons to electrons by a photovoltaic cell. It is defined as the number of electrons in the external circuit produced by an incident photon at a given wavelength divided by the number of incident photons. IPCE measurements were taken for the three DSSC systems, (A) SnO_2/dye/electrolyte/Pt, (B) SnO_2-MgO/dye/electrolyte/Pt and (C) Au@SnO_2-MgO/dye/electrolyte/Pt using the three respective photoanodes described above. Experimental setup consisted of monochromatic light illumination from a Bentham PVE300 unit equipped with a TMC 300 monochromator-based IPCE system with a 150 W xenon arc lamp covering the 300 nm –1100 nm wavelength range. For comparison purposes, the UV–VIS absorption spectra of the MgO incorporated SnO_2 electrodes and the Au NP incorporated SnO_2: MgO photoanode films were also taken. For these measurements films of bare SnO_2, SnO_2:MgO and Au: SnO_2:MgO spayed on FTO glass plate were used. After sintering at 550 °C for 45 min., and after cooled down to room temperature, the films were used to obtain the optical absorption curves for the determination of the corresponding energy band gap values. All optical absorption measurements were done using a Shimadzu 2450 UV–VIS spectrophotometer in the wavelength range of 300–800 to nm.

2.8. Dye adsorption in photoanode

The amount of dye adsorption by the three photoanodes, bare SnO_2, SnO_2:MgO and SnO_2:MgO were estimated by desorbing the dye in 0.1 M NaOH aqueous solution and then measuring the optical absorbance of the dye desorbed NaOH solution using the colorimetry technique. This method is generally used to determine the concentration of colored compounds in solutions by the application of the Beer–Lambert law, which states that the concentration of a solute is proportional to the absorbance. The absorption measurements were done using a Shimadzu 2450 UV–Vis spectrophotometer in the wavelength range of 200 nm–1100 nm.

2.9. EIS measurements

In order to see the effects of the MgO insulator layer incorporated SnO_2 electrode and the Au NP incorporated SnO_2:MgO photoanode on the electron life time and the interfacial charge-transfer resistance, R_{CT2}, Electrochemical Impedance Spectroscopy (EIS) measurements were performed on the DSSCs using a Metrohm Autolab Potentiostat/Galvanostat PGSTAT 128 N with a FRA 32 M Frequency Response Analyzer (FRA) covering the 1 MHz–0.01 Hz frequency range. These measurements were carried out under the illumination of 100 mW cm^{-2} using the same solar simulator that was used for I–V measurements.

3. Results and discussion

3.1. Optical absorption of gold nanoparticles and dye

The UV–VIS optical absorption spectra of the Au NP colloidal suspension and the N719 dye are shown in Fig. 5 (b). As seen from Fig. 5 (b), the absorption spectra of the Au colloids exhibit a broad surface plasmon resonance absorption band with the maximum around 530 nm. From the position of this absorption maximum, it can be estimated that the diameters of the gold nanoparticles are in the 30 – 35 nm range (Njoki et al., 2007). The TEM and EDX image confirms the presence and Size of Au NPs we have used in this study in Fig. 4, This was confirmed size of that the AuNP size range was 30 – 35 nm. Fig. 6.

Further, this was confirmed by the particle size analyzer measurements using the Dynamic Light Scattering method (DLS). The average particle size determined by this method was 42.0 nm. It should be mentioned here that the DLS measures the size and size distribution of particles in solution and the size determined by DLS is typically greater than that ascertained by Transmission Electron Microscopy due to the fact DLS gives the hydrodynamic size which takes into consideration the core size of the gold nanoparticles as well as the shell of water surrounding it.

As the size or the shape of the nanoparticles varies, the observed color also changes. Gold nanospheres prepared in this work have a characteristic wine-red colour as shown in Fig. 4(a). It is generally accepted that the color of the metal nanoparticles is due to the collective surface plasmon oscillations of the electrons in the conduction band. The oscillation frequency is usually in the visible region for gold giving rise to the strong surface plasmon resonance absorption (Dissanayake et al., 2016; Hägglund et al., 2008). Although the conduction and valence bands of semiconductors such as SnO_2 are separated by a well-defined band gap, metal nanoparticles have close-lying

bands where electrons can move quite freely. These free electrons give rise to surface plasmon-absorption bands in metal NPs, which depends on both the particle size and the chemical surroundings.

The free electrons in the metal (*d* electrons in Au) are free to travel through the material and all interactions are expected to be confined to the surface. When the wavelength of light is much larger than the nanoparticle size, it can set up standing resonance conditions. Light in resonance with the surface plasmon oscillation causes the free-electrons in the metal to oscillate. As the wave front of the light passes, the electron density in the particle gets polarized to one surface and oscillates in resonance with the light's frequency causing a standing oscillation. Under this local surface plasmon resonance (LSPR) condition, enhanced light absorption occurs which depends on the types, sizes, shapes, and the dielectric constants of the metal and the surrounding medium.

3.2. Optimization of SnO_2 layer thickness and MgO amount

Fig. 7 shows the efficiencies of the N719 dye sensitized solar cells fabricated with different thicknesses of bare SnO_2 based photoanodes. Since the amount of the precursor dispersion, height of the spray gun from the hot plate and the spraying time were fixed, the amount of material deposited on the substrate and the thickness of the SnO_2 film increases with the decreases of the effective area of the SnO_2 film (i.e. number of substrates cells per series).

The increase in the sprayed area along the x-axis in Fig. 7 was assumed to be inversely-proportional to the thickness of the SnO_2 film. As it is evident from this Figure, DSSC made with the photoanode prepared by spraying 6 cells per set (volume of precursor dispersion was 40

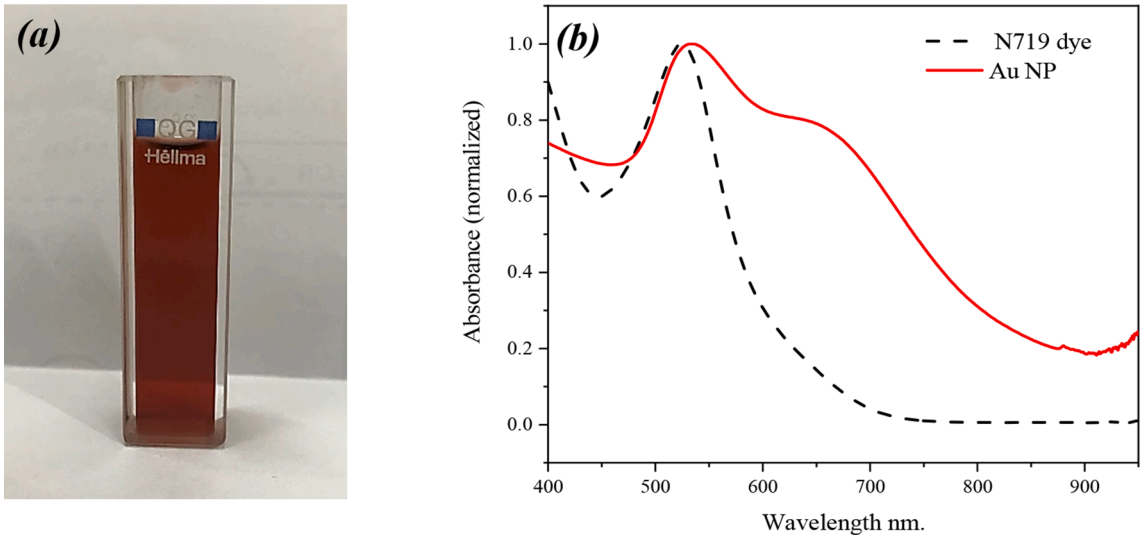

Fig. 5. (a) Image of colloidal Gold nanoparticles (wine red colour) and **(b)** Absorbance spectra of N719 dye (black colour, dash line) & colloidal Au NPs (Red colour, Solid line). (For interpretation of the references to color in this figure legend, the reader is referred to the web version of this article.)

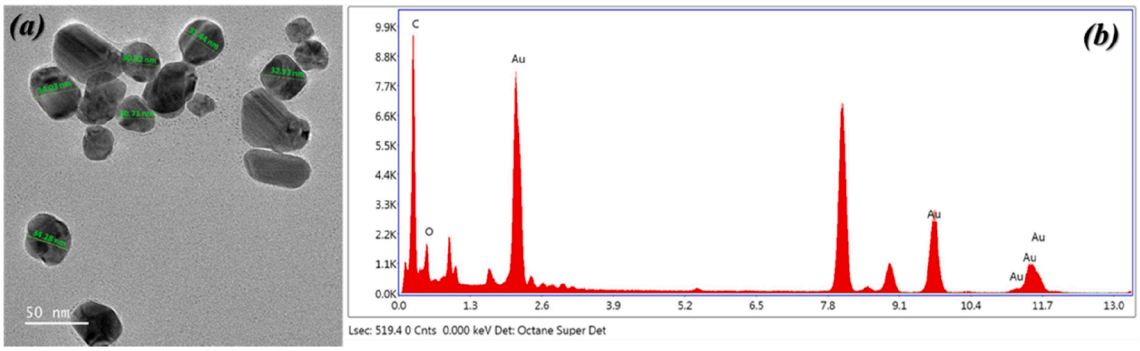

Fig. 6. (a) TEM image of AuNP and (b) EDX graph of prepared colloidal AuNP.

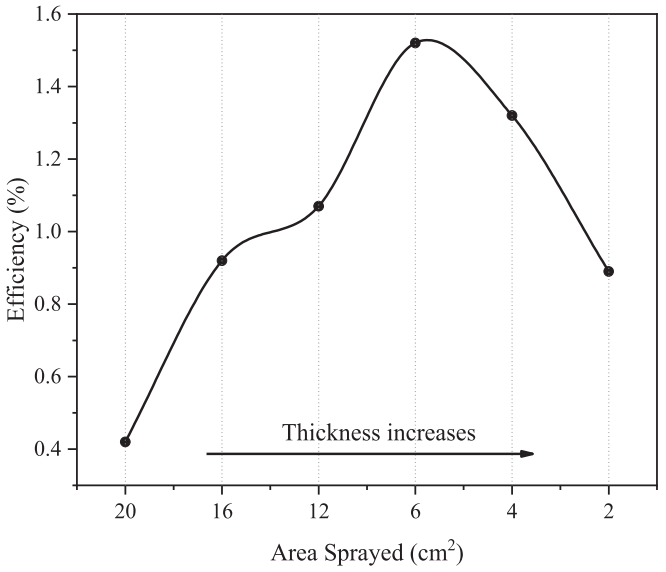

Fig. 7. Efficiency variation of the DSSCs with the sprayed area corresponding to SnO_2 film thickness.

ml, height of the spray gun from the hot plate was approx. 35 cm, spraying time duration was 12 to 15 min) has given the highest efficiency of 1.52%. Beyond this optimum thickness of the photoanode, the efficiency of DSSC decreases with increasing film thickness of the photoanode. Corresponding *I–V* characteristics data such as short circuit photocurrent density (J_{SC}), open circuit voltage (V_{OC}), fill factor (*FF*), and the efficiency (η %) of these DSSCs are tabulated in Table 1 with respect to their sprayed area while the volume of precursor dispersion, height of the spray gun from the hot plate and the spraying time duration were kept unchanged. When the thickness of the SnO_2 film of fixed cell area increases initially, the effective total surface area available for dye adsorption also increases. Because of this, the generation of photoelectrons and the corresponding photocurrent also increase resulting an increase in the efficiency (O'Regan and Grätzel, 1991; Gong et al., 2017). However, as shown in Fig. 7, the efficiency decreases after reaching the optimum film thickness. The SEM cross-sectional view (Fig. 8) shows the optimum thickness of photoanode, which is around 12.0 μm. As depicted in Fig. 1 by the graphical picture, the composite structure is not a typical double layer structure with two distinct layers but it is a predominant SnO_2 layer with most SnO_2 particles coated with nanosize MgO.

Table 1
Photovoltaic parameters of DSSCs made with different SnO_2 photoanode thicknesses. These correspond to different sprayed areas where the volume of precursor dispersion, height of the spray gun from the hot plate and the spraying time duration were kept unchanged. Each cell area was 25 cm^2.

Sprayed active area	V_{OC} (mV)	J_{SC} (mA cm^{-2})	*FF* (%)	Efficiency (%)
20 cm^2 (20 cells per set)	381.1	2.17	50.54	0.42
16 cm^2 (16 cells per set)	401.8	4.21	54.2	0.92
12 cm^2 (12 cells per set)	398.6	4.84	55.6	1.07
6 cm^2 (06 cells per set)	452.2	6.07	55.2	1.52
4 cm^2 (04 cells per set)	394.1	6.33	52.9	1.32
2 cm^2 (02 cells per set)	392.1	4.27	53.0	0.89

In these solar cells, even though the amount of dye adsorption increases with photoanode film thickness, the overall film resistance and the rate of electron recombination also increase resulting a decrease in the photocurrent, as observed and reported also by other groups (Senadeera et al., 2018; Kumari et al., 2016). Based on these observations, it was found that the DSSCs made with SnO_2 based photoanodes prepared by spraying 6 cells per set exhibit the best solar cell performance and these solar cells were used in this work for further studies. In order to obtain the optimum amount of MgO incorporated into the SnO_2 photoanode, the different weight percentages of MgO as shown in Table 2 were used to prepare the SnO_2:MgO photoanodes. DSSCs were fabricated with these photoanodes and characterized using the same method as described under section 2.4. Table 2 shows the short circuit photocurrent density (J_{SC}), open circuit voltage (V_{OC}), fill factor (FF), and the efficiency (η %) of all these DSSCs with respect to the ww% of MgO.

Fig. 9 shows the V_{OC}, J_{SC} and η variation of DSSCs vs the MgO weight percentage. According to Fig. 9, the variation of MgO wt% gives a sharp peak for J_{SC}, when the MgO wt% is equal to 4.6%, and thereafter the J_{SC} decreases rapidly. This is because, beyond the optimum ww% of MgO, the thicker insulator MgO layer blocks the forwarding electrons too.

According to Tennakone et al (Tennakone et al., 2001), the photo-excited dye on the outer MgO layer on SnO_2 could tunnel electrons to the conduction band of the SnO_2. When the film thickness of MgO layer is very thin, the direct tunnelling transfer will be more feasible. However, when the MgO film thickness increases beyond the optimum value, the V_{OC} will be increased but the insulating nature of the thicker MgO layer will limit the electron tunnelling. Hence, J_{sc} will decrease showing a weaker photovoltaic performance. The maximum efficiency of 4.13 % was obtained at 4.6 MgO wt% which also corresponds to the maximum value of J_{SC}. Corresponding *J-V* curves are shown in Fig. 9. As it can be seen from Fig. 11, (*J-V* curve −1 and curve −2), a dramatic enhancement of V_{OC}, J_{SC} and fill factor can be observed and hence the efficiency in the DSSCs corresponding to the optimized SnO_2:MgO photoanode. The increase in the fill factor from 55.2% to 72.4% in the optimized DSSC proves the effectiveness of the MgO layer in reducing the electron recombination. Based on these observations, the SnO_2:MgO based photoanodes prepared with 4.6% of MgO showing the best solar cell performance was used for further studies.

3.3. Efficiency enhancement by plasmonic effect by Au nanoparticles

DSSCs were fabricated using optimized SnO_2:MgO photoanodes

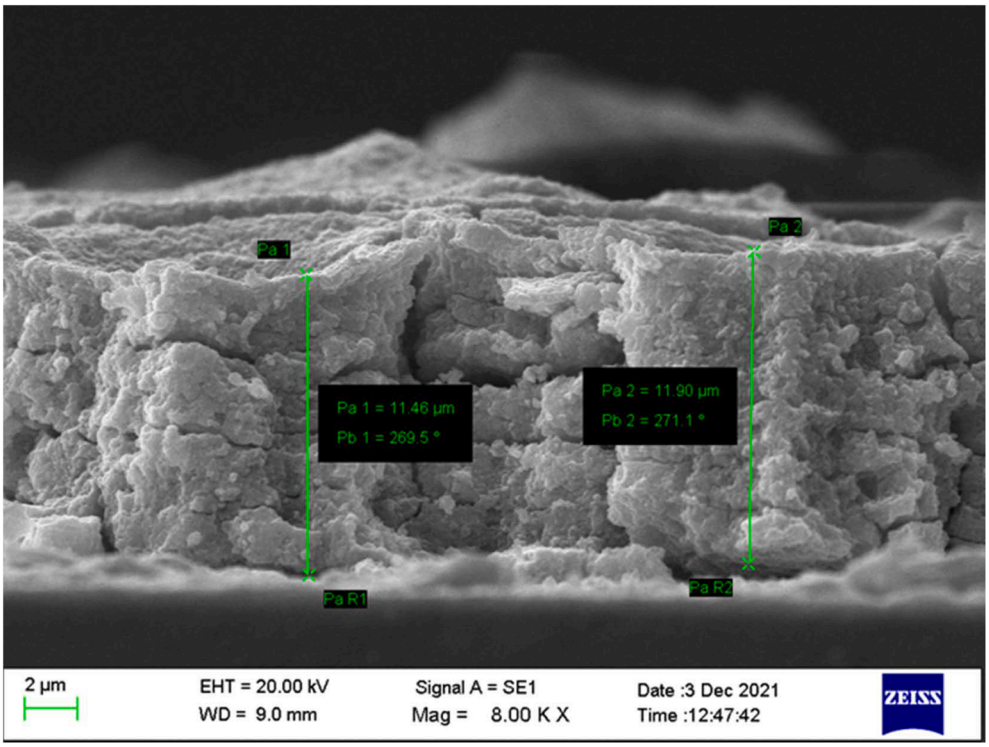

Fig. 8. Cross-section of thickness optimized photoanode.

Table 2
Photovoltaic parameters of DSSCs with respect to the ww% of MgO.

Photoanode	MgO (ww %)	V_{OC} (mV)	J_{SC} (mA cm^{-2})	*FF* (%)	Efficiency (%)
SnO_2	0.0	452.2	6.07	55.22	1.52
SnO_2 / MgO	3.8	642.8	6.91	67.90	3.01
	4.6	**715.8**	**7.98**	**72.35**	**4.13**
	5.1	746.5	6.56	72.12	3.53
	8.0	768.7	5.95	74.94	3.43
	10.0	784.0	5.35	75.05	3.15
	12.0	794.5	4.90	77.41	3.01

incorporating different amounts of gold colloidal suspension containing gold nanoparticles (Au NPs) as explained in section 2.3. Fig. 10 shows the variation of photocurrent density and the efficiency with the amount of Au NPs incorporated into the SnO_2:MgO photoanode. Both the J_{SC} and the efficiency exhibit the maxima corresponding to the concentration of 0.3 ml Au NP colloidal solution incorporated into the SnO_2:MgO photoanode.

The initial increase in the J_{sc} and the efficiency is clearly due to the enhanced light absorption by the plasmonic gold NPs due to LSPR effect which increases with the number of Au NPs incorporated into SnO_2:MgO electrode. Subsequently, a competing mechanism starts to dominate when the amount of incorporated Au NPs increases beyond the optimum concentration of 0.3 ml colloidal solution. At these concentrations, a large number of Au NPs could reside inside the composite SnO_2:MgO grains rather than residing them at the surface of these crystallites and thereby increasing the parasitic absorption, which does not contribute to the photo-generation of electron/hole pairs. This parasitic absorption significantly hinders the plasmonic effect and ultimately decreases the photocurrent and the efficiency of the DSSC after reaching the optimized concentration of NPs (Dissanayake et al., 2020; Rand et al., 2004; Umair et al., 2020). The *I-V* characteristics of DSSCs with different amount of Au NPs are shown in Table 3. In these plasmoinc DSSCs, both J_{SC} and efficiency gradually increases and reaches the maxima at 9.06 mA cm^{-2} and 4.69%, respectively, corresponding to the Au NP content of 0.3 ml colloidal solution.

3.4. Photovoltaic performance of DSSCs

J-V characteristics of the DSSC fabricated with optimized Au NP in the optimized SnO_2:MgO composite photoanode measured under the same illumination condition as above is also shown in the Fig. 11 (Curve – 3). Table 4 summarizes the corresponding photovoltaic parameters. These observations suggest that electron transfer from the excited dye attached to the SnO_2:MgO oxide surface to the underlying SnO_2 occurs by tunneling through the MgO insulator layer. As mentioned in the introduction, since a thin MgO insulating layer is formed around each SnO_2 semiconductor particle in the photoanode, it remarkably and effectively reduces the recombination of the photo-generated electrons from the excited dye molecules. This has resulted a dramatic enhancements in J_{SC} from 6.07 to 7.98 mA cm^{-2}, V_{OC} from 452.2 to 715.8 mV, *FF* from 55.22 to 72.35% and the efficiency from 1.52% to 4.13% solely due to the incorporation of the MgO layer to form the SnO_2:MgO composite photoanode (Fig. 11, curves 1 and 2 and Table 4). These findings are in agreement with the results reported for the first time by Tennakone et al. for a DSSC with SnO_2:MgO photoanode. There are two major recombination processes present in DSCs. One is the regeneration of excited dye molecules with the injected electrons. The other is the combination of the injected electrons with the triiodide ions in the electrolytes due to the back tunneling of injected electrons. As discussed earlier, this effect arises due to the impressive inhibition of electron back transfer from SnO_2 to the redox electrolyte (I_3^-) by the MgO insulating layer (Tennakone et al., 2001; Sewvandi et al., 2014). The optimum MgO layer thickness is expected to be around few angstroms, suggesting that electron transfer from the excited dye attached to the MgO oxide surface to the underlying SnO_2 occurs by tunnelling through the thin insulator layer. Table 4 shows that even the plasmonic effect in the DSSCs appears to be greatly enhanced due to the presence of the MgO layer.

It should be noted that, as seen from the Table 4, the enhancements in J_{sc}, V_{oc} and efficiency due to the plasmonic effect in Au@ SnO_2 photoanode, without the presence of MgO layer is not so significant.

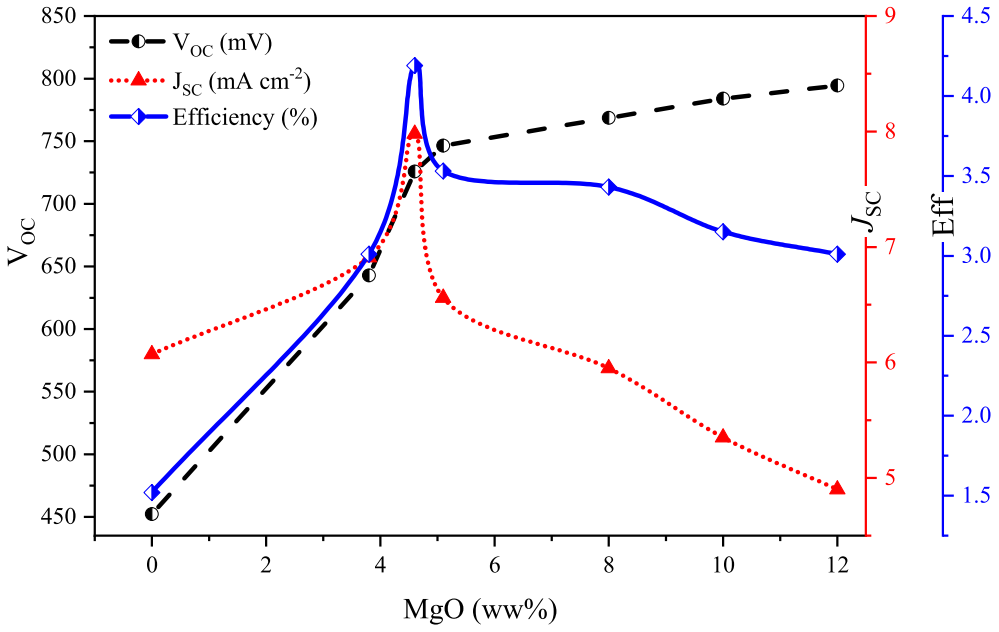

Fig. 9. Open-circuit Voltage, Photocurrent Density and Efficiency variation of the DSSCs with respect to the ww% of MgO.

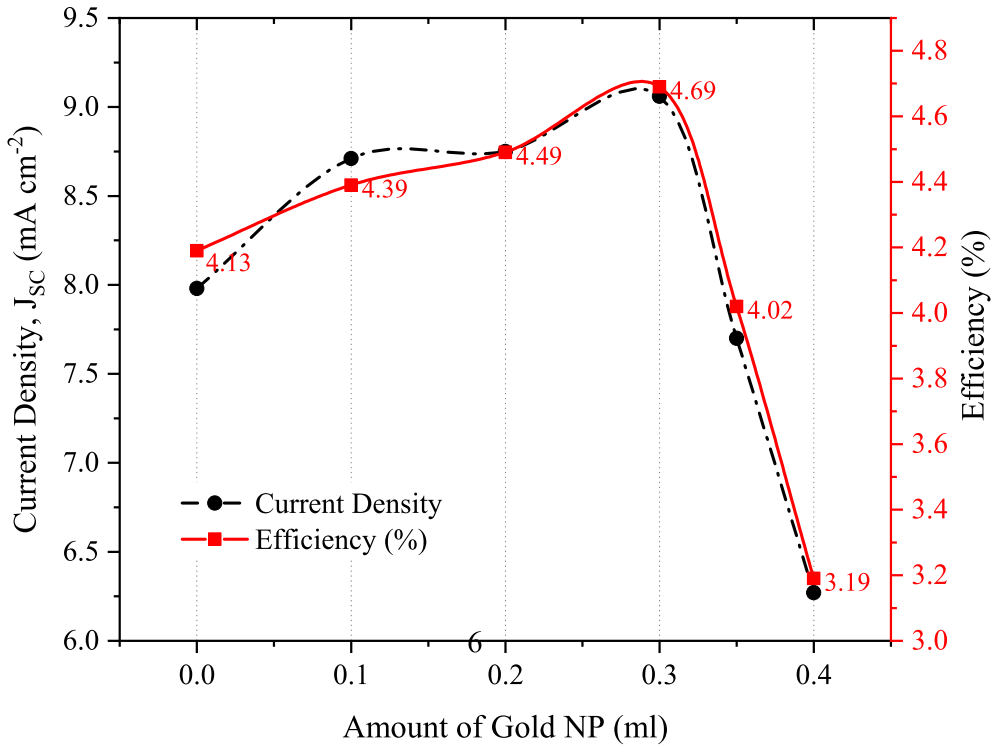

Fig. 10. Photocurrent density and efficiency variation of the DSSCs with respect to the amount of Au NP colloidal solution incorporated in SnO_2:MgO photoanode.

However, the presence of Au NPs in the Au@ SnO_2:MgO composite photoanode has significantly increased the J_{sc} further from 7.98 to 9.06 mA cm^{-2} while the enhancement in V_{OC} is from 715 to 725 mV highlighting the enhanced photoelectron generation by the plasmonic effect. Similar results of enhanced J_{sc} values due to plasmon-induced photoelectron generation are reported for the plasmonic DSSCs incorporating gold and silver nanoparticles in SnO_2 and TiO_2 based and Quantum dot sensitized photoanodes (Dissanayake et al., 2020; Dissanayake et al., 2016; Hägglund et al., 2008; Rand et al., 2004; Umair et al., 2020).

The combined effect of the presence of the MgO insulating layer and the Au NPs in the composite photoanode has shown a dramatic increase of J_{sc} from 6.07 to 9.06 mA cm^{-2} representing a remarkable 49% enhancement in J_{sc}. The corresponding enhancement in the DSSC efficiency from 1.52 % to 4.69 % represents a remarkable 209 %.

By comparing the performance of the two photoanodes (1) and (2) in Table 4, it is clear that the plasmonic effect due to Au NPs have increased the J_{sc} only by 5.4%. However, a comparison of the two photoanodes (3) and (4) shows that the increase in J_{sc} due to plasmonic effect is 13.5 % confirming that the presence of the MgO layer in the SnO_2 photoanode have strengthened the plasmonic effect also, in addition to inhibiting the

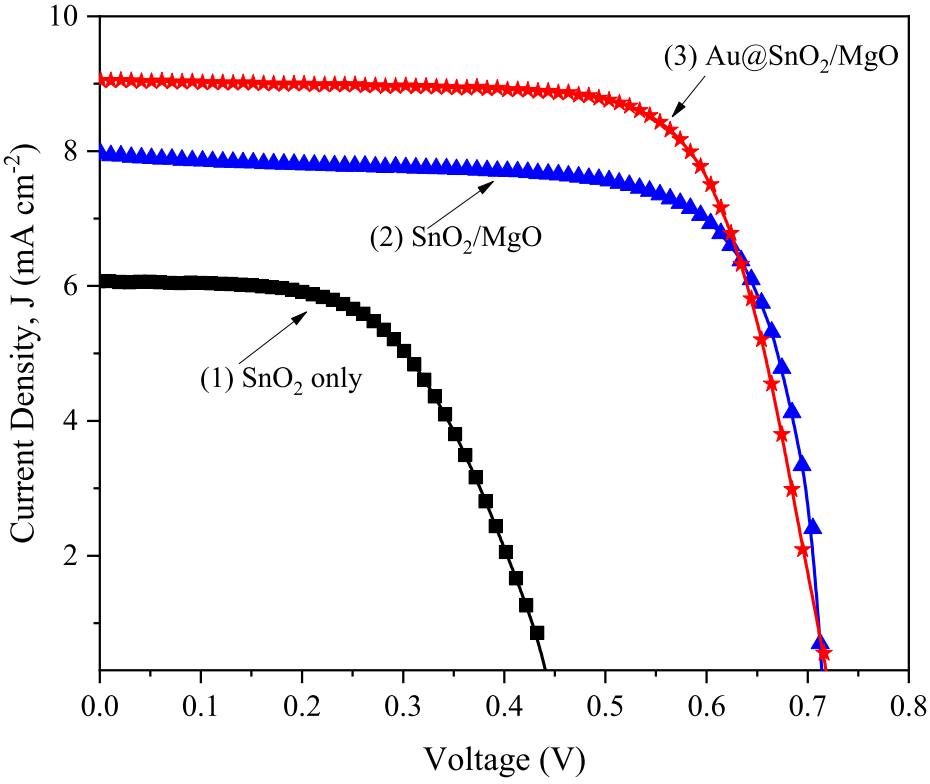

Fig. 11. J-V characteristics of the DSSCs made from (1) bare SnO_2 film (Square, Black symbol),(2) SnO_2:MgO film(Triangle, Blue symbol) and (3) AuNP incorporated SnO_2:MgO film (Star, Red symbol). (For interpretation of the references to color in this figure legend, the reader is referred to the web version of this article.)

Table 3
I-V characteristics of plasmonic DSSCs made with Au NP incorporated SnO_2: MgO photoanodes as a function of the added amounts of gold nanoparticles (Au NP).

Cell	V_{OC} (mV)	J_{SC} (mA cm^{-2})	*FF* (%)	Efficiency (%)
SnO_2/ 4.6% MgO	715.8	7.98	72.35	4.13
SnO_2 / MgO/ 0.1 ml Au NP	712.4	8.71	70.77	4.39
SnO_2 / MgO/ 0.2 ml Au NP	718.8	8.75	71.52	4.49
SnO_2 / MgO/ 0.3 ml Au NP	**725.6**	**9.06**	**71.36**	**4.69**
SnO_2 / MgO/ 0.35 ml Au NP	719.9	7.70	72.51	4.02
SnO_2 / MgO/ 0.4 ml Au NP	707.9	6.27	71.81	3.19

Table 4
Photovoltaic parameters for DSSCs made with different photoanodes: (1) bare SnO_2 (2) AuNP incorporated SnO_2, (3) SnO_2:MgO composite and (4) AuNP incorporated SnO_2:MgO composite.

Photoanode	V_{OC} (mV)	J_{SC} (mA cm^{-2})	FF (%)	Efficiency (%)
(1) SnO_2 only	452.2	6.07	55.22	1.52
(2) Au@ SnO_2	454.5	6.40	56.44	1.64
(3) SnO_2:MgO	715.8	7.98	72.35	4.13
(4) Au@ SnO_2:MgO	725.6	9.06	71.36	4.69

back electron transfer.

We have done some stability tests of these solar cells by monitoring the J_{sc} and V_{oc} over a period of 50 h. It was observed that both J_{sc} and V_{oc} decreased gradually to about 85% of their original values during this time period. As these tests were not done under perfect sealed conditions this poor stability appears to be due to acetonitrile based electrolyte evaporation and moisture absorption.

3.5. Incident photons to current conversion efficiency (IPCE) analysis

The effectiveness of a dye-sensitized cell to convert light of various wavelengths into electrical energy is measured by the incident photons to current conversion efficiency (IPCE) defined as the number of electrons generated by light per number of photons incident on the cell. The IPCE measures how efficiently the solar cell converts the incident photons into current at a given wavelength. Results of IPCE measurements taken for the three DSSC systems: (A) SnO_2/dye/liquid electrolyte/Pt, (B) SnO_2-MgO/dye/liquid electrolyte/Pt, and (C) Au@SnO_2-MgO/dye/liquid electrolyte/Pt, using Ru N719 as the sensitizing dye under the same illumination condition are shown as in Fig. 12. The highest IPCE values were observed for the DSSC made with Au: SnO_2:MgO photoanode for incident light covering almost the entire visible wavelength range.

The IPCE peak heights are 41.5% at 524.1 nm for DSSC with SnO_2: MgOand 42.7% at 524.9 nm for DSSC with Au:SnO_2:MgODSSC. Both these are much higher than the peak height of 31.8% at 511.6 nm for DSSCs made with reference photoanode, SnO_2 clearly confirming the effect of MgO layer in the photoanode in minimizing the back electron transfer and the plasmonic effect by Au NPs in enhancing the light absorption by LSPR effect and thereby increasing the overall short circuit photocurrent density. Additionally, the current density (J_{SC}) was calculated from IPCE data. Integrated J_{SC} value of bare SnO_2, SnO_2:MgO composite and AuNP incorporated SnO_2:MgO composite were 6.12 mA cm^{-2}, 8.30 mA cm^{-2}, 9.18 mA cm^{-2} respectively.

3.6. Dye adsorption by the photoanode

It is well known that the amount of dye adsorbed on the photoanode semiconductor layer significantly affects the short circuit current density and hence the power conversion efficiency of a DSSC. The estimated

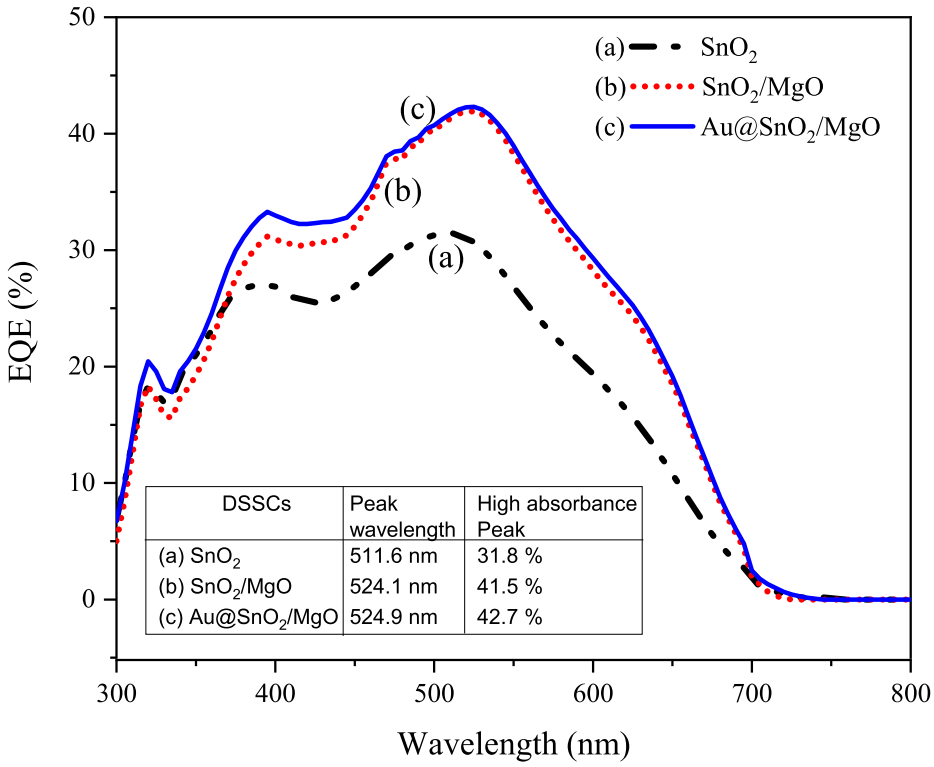

Fig. 12. Comparison of spectral responses (IPCE) of DSSCs made with photoanodes: (a) Bare SnO_2, (b) SnO_2:MgO composite and (c) Au NP incorporated Au:SnO_2:MgO composite.

amounts of dye adsorption in above three types of photoanodes, (a) bare SnO_2, (b) SnO_2:MgO composite and (c) AuNP incorporated Au: SnO_2:MgO composite are shown in the Table 5. The lowest dye adsorption of 1.73×10^{-7}mol cm^{-2} was achieved by the pristine SnO_2 photoanode and other photoanodes shows higher values. It is well known that N719 dye adsorbed on the semiconductor surface by forming a monolayer. Therefore, it is expected that a lower dye loading will result a lower short-circuit photocurrent density. However, in the case of Au: SnO_2:MgO photoanode, the dye loading is lower but the J_{SC} is higher compared to the SnO2:MgO photoanode. This could be due to the occupation of some sites on the SnO_2:MgO surface by Au NPs thereby limiting the available sites for dye loading in the plasmonic photoanode. Therefore, the J_{SC} enhancement exhibited by Au: SnO_2:MgO based DSSC is evidently due to the dominating local surface plasmon resonance (LSPR) effect at the expense of lower dye loading.

3.7. Flat-band potential measurements by Mott-Schottky plots

The enhancement of photovoltage and the photocurrent due to the formation of the thin MgO layer around SnO_2 semiconductor grains and also the incorporation of Au NPs into the SnO_2 semiconductor surface can be described by the rise of the conduction band edge of the semiconductor due to the formation of Schottky junction at the insulator/ semiconductor interface and the metal/ semiconductor interface. The shift of the conduction band edge due to these two processes has been estimated using Mott-Schottky measurements. Fig. 13 shows the Mott-schottky plots of (1) bare SnO_2film, (2) SnO_2:MgO composite film and (3) Au: SnO_2:MgO composite film deposited on FTO glass.

Table 5
The amount of dye loading on the three photoanodes: (a) prestine SnO_2, (b) SnO_2:MgO composite and (c) Au NP incorporated composite.

DSSC Photoanode	Dye Loading density / mol cm^{-2}	J_{SC} / mA cm^{-2}
(a) SnO_2 only	1.73×10^{-7}	6.07
(b) SnO_2:MgO	7.12×10^{-7}	7.98
(c) Au:SnO_2:MgO	7.00×10^{-7}	9.06

This Figure clearly indicates that the conduction band edge of the SnO_2:MgO film has shifted up by ~0.200 eV compared to bare SnO_2 film and also the conduction band edge of the gold incorporated Au:SnO_2:MgO film has shifted up by ~0.012 eV compared to SnO_2:MgO film (Table 6). The open-circuit voltage depends on the height of the electron quasi-fermi level (QFL) and it is more sensitive to electron recombination. The difference between the electron QFL in the SnO_2 and the redox potential of the electrolyte gives the V_{OC} of the DSSC. The V_{OC} of a SnO_2 based DSSCs is around 350 mV to 450 mV. This V_{OC} could be increased by 200 mV to 300 mV through the coating of MgO on the SnO_2 particles. As suggested, the QFL has risen even above the bottom of conduction band level (Tennakone et al., 2001).

As reported by Hagfeldt et al (Hagfeldt et al., 1994) and Aponsu et al (Aponsu et al., 2010) the situation of a interface between a nano size metal particle and a semiconductor is rather different from an interface between a micro size metal particle and a semiconductor interface. When an n-type semiconductor is in contact with a higher work function metal, electrons in the conduction band of the semiconductor are transferred to the metal. The density of free carriers in the semiconductors are usually low, and hence, free carriers lying in the semiconductor from the surface to the deep bulk must be transferred to the metal in order to line up with the Fermi levels.

As a consequence, bands of semiconductor bend at the interface forming a depletion layer, which could extend even to a depth of one micrometer. However, the situation is rather different at a metal/ semiconductor interface when the particles are of nano size. In this situation, a build up of a depletion layer at the interface is questionable because of the small size of the semiconductor and the metal particles. However, still their energies have to be equalized when they are in contact. Therefore, electrons in the material with higher Fermi level have to transfer to material with lower Fermi level even these particles are in nano scale. The Fermi level of SnO_2 is higher compared to the Fermi level of gold. Therefore, electrons in the conduction band of SnO_2

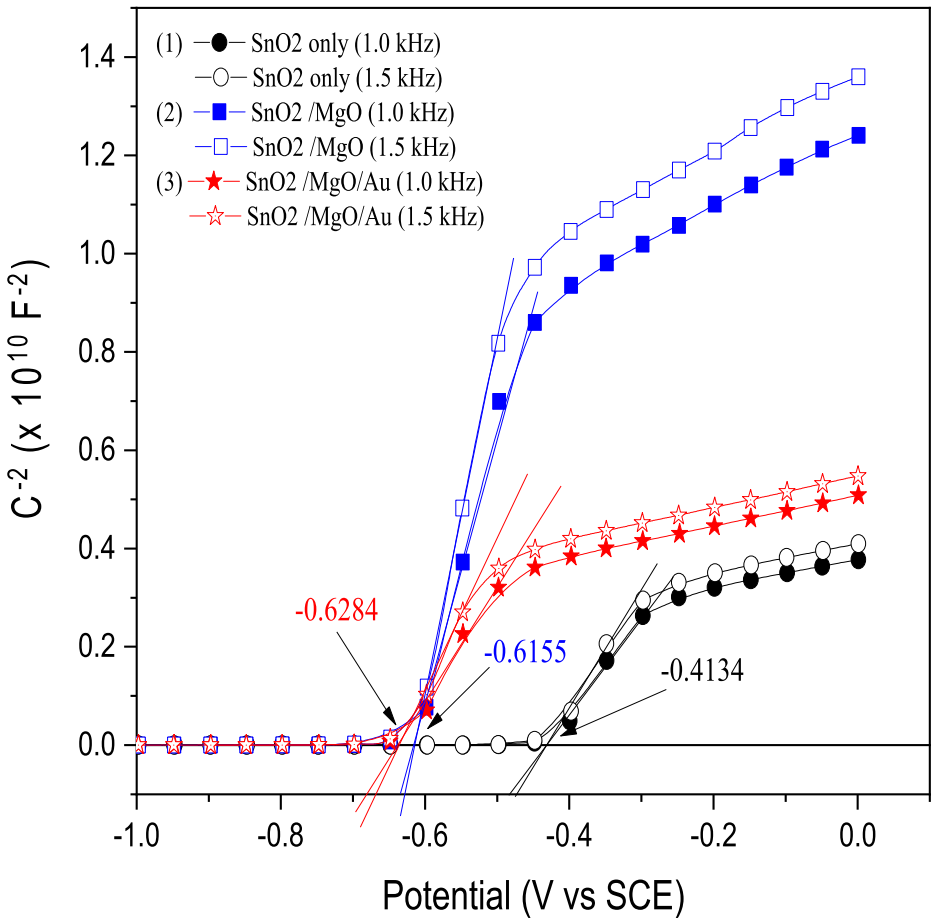

Fig. 13. Mott-Schottky plots of (1) bare SnO_2 (1.0 kHz & 1.5 kHz), (2) SnO_2:MgO composite (1.0 kHz & 1.5 kHz) and (3) Au:SnO_2:MgO (1.0 kHz & 1.5 kHz) photoanodes.

Table 6
Flat band potential (V_{FB}) values of the three photoanodes: (1) bare SnO_2, (2) SnO_2:MgO composite and (3) Au:SnO_2:MgO composite and the V_{OC} values of the corresponding DSSCs.

Photoanode	V_{FB} with respect to SCE (V)	V_{OC} (mV)
(1) SnO_2	−0.4134	452.2
(2) SnO_2:MgO	−0.6155	715.8
(3) Au:SnO_2:MgO	−0.6284	725.6

get transferred to gold to gain an equilibrium energy state. Since the particles are in nano range the potential of the conduction band edge of SnO_2 rises up together with the shallow traps and the Fermi level of the Au:SnO_2:MgO composite (Aponsu et al., 2010; Hagfeldt et al., 1994; Ramakrishna et al., 2004).

The magnitude of the photovoltage (V_{OC}) represents the energy difference (ΔE) between the apparent Fermi level ($E_F^{'}$) of the semiconductor film and the reduction potential (E^{o}_{redox}) of the redox couple (I^-/I_3^-) in the electrolyte,

$$VOC = \Delta E = E_F^{'} - E^{o}_{redox}$$

According to the results of our flat band potential measurements (Table 6 and Fig. 13), the apparent Fermi level ($E_F^{'}$) has shifted to more negative values for the SnO_2:MgO composite film and Au NP incorporated SnO_2:MgO films compared to the reference SnO_2film. This is consistent with the enhancement of V_{OC} values of the DSSCs as observed from their I–V characteristics (Table 4 and Table 6). A similar shift in apparent Fermi level and anincrease in the photovoltage as has been reported for the DSSCs with Au incorporated bare SnO2 (Zainudin et al., 2019; Aponsu et al., 2010).

3.8. XRD analysis and TEM

Figure 14A A shows the powder XRD patterns of bare SnO_2, SnO_2: MgO and Au:SnO_2:MgO prepared for photoanodes after sintered at 550 °C. All the diffractions are assigned to the crystalline phase of tin oxide. The XRD pattern is in excellent agreement with the reference pattern of tin oxide nanoparticles. SnO_2 has dominant peaks at 110, 101, 200, 111, 211, 220, 002. The major peak of MgO at $2\theta = 43°$ (200). This is hardly visible in the XRD spectrum of SnO_2:MgO and Au:SnO_2:MgO, because SnO_2 also has a peak at 43°. This we believe is due to the insufficient amount of MgO present in the structure. Tennakone *et al* also mentioned the same but confirmed the presence of MgO in their samples by gradually increasing the MgO% (Tennakone et al., 2001). Therefore, we believe that MgO thin film coating is present in the structure prepared by us also as we have used the identical preparation procedure, but not prominent peak due to insufficient amount of MgO. However, the mixture containing higher concentration (50%) than the optimized amount of MgO clearly showed the presence of MgO (Fig. 14B).

Tennakone *et al* also mentioned the same and confirmed the presence of MgO by increasing the MgO%. However, the presence of MgO in the SnO_2: MgO film prepared by us after sintering is further confirmed by TEM shown here (Fig. 15). According to our TEM the d-values are SnO_2 = 0.33 nm (The d-spacing of SnO_2 structure is 0.33 nm corresponding to the (110) planes) and MgO = 0.21 nm. Theese d- values are in agreements with Patel, M. et al and Haddad, N at el. The presence of SnO_2 (d = 0.33 nm) and MgO nanoparticle (d = 0.21 nm) (Patel et al., 2013; Haddad et al., 2017).

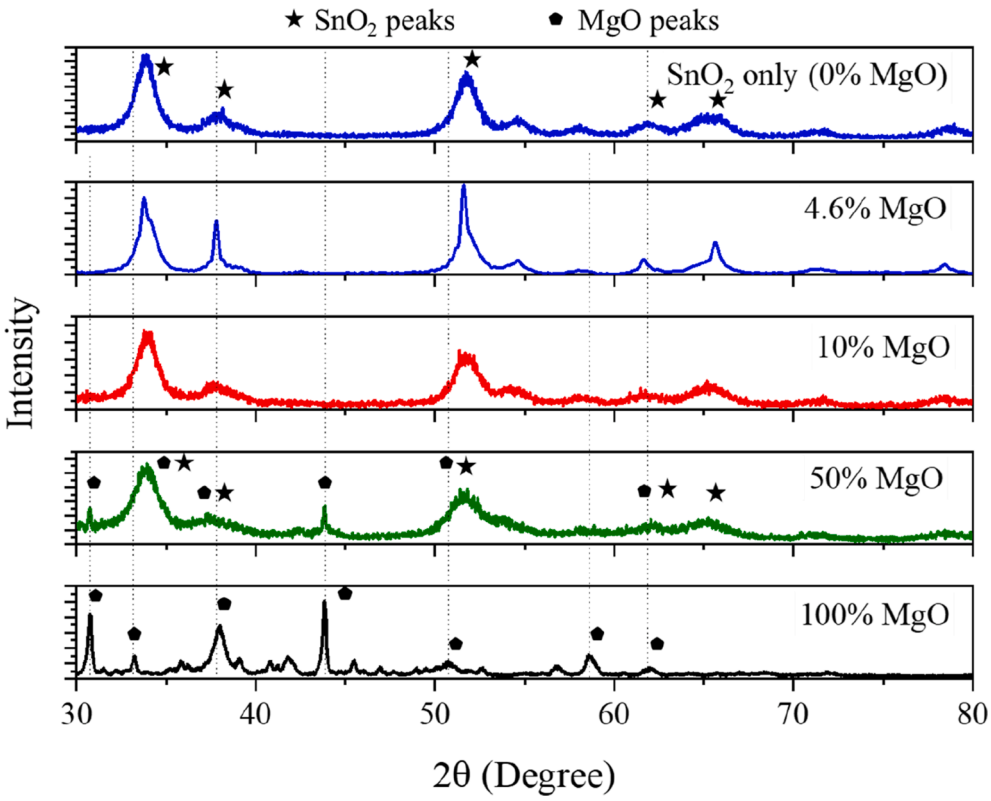

Fig. 14A. Powder X-ray diffraction patterns of bare SnO_2, SnO_2:MgO and Au:SnO_2:MgO powder samples.

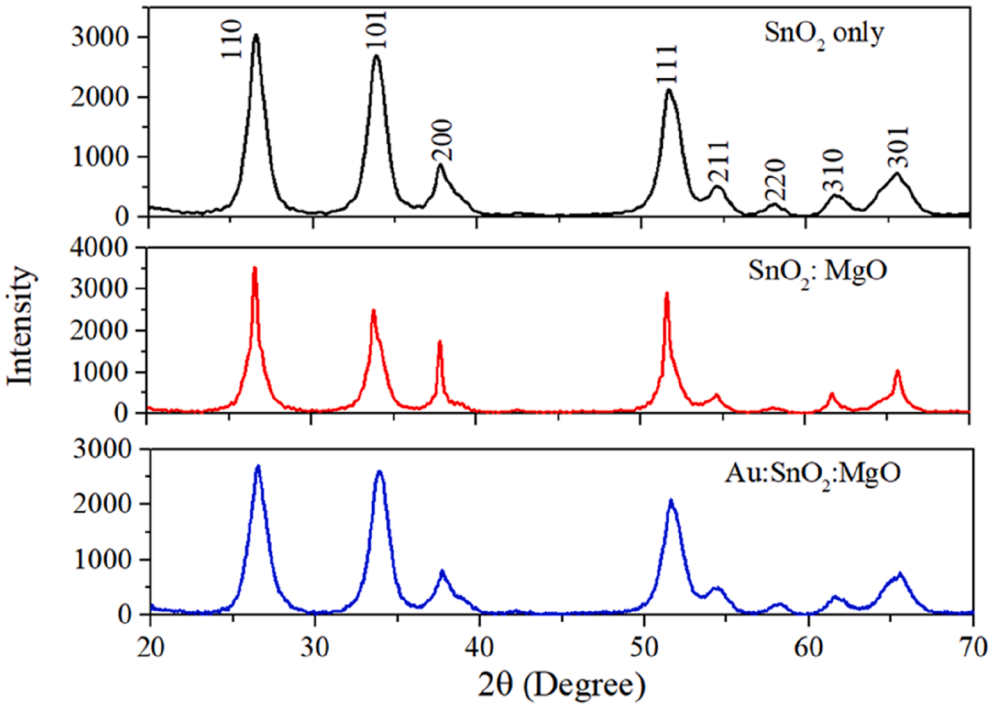

Fig. 14B. XRD characterization of different concentrations of MgO in the mixture.

3.9. EIS analysis

Fig. 16 (a) shows the Nyquist plots of the electrochemical impedance spectra of DSSCs made with bare SnO_2, SnO_2:MgO and Au:SnO_2:MgO photoanodes measured in the frequency range from 1 MHz to 0.01 Hz. Each Nyquist plot displays a series resistance R_S which occurs in the high frequency region (near1 MHz) and from left to right, three semicircles appear in decreasing order of the frequency; These represent, (i) charge transfer at platinum counter electrode/redox electrolyte interfaces (R_{Pt}, above 1 kHz); (ii) charge transfer resistanceand recombination resistance at the photoanode/electrolyte interface (R_{CT}, between 1 Hz and 1 kHz); and (iii) electron diffusion resistance through photoanode and

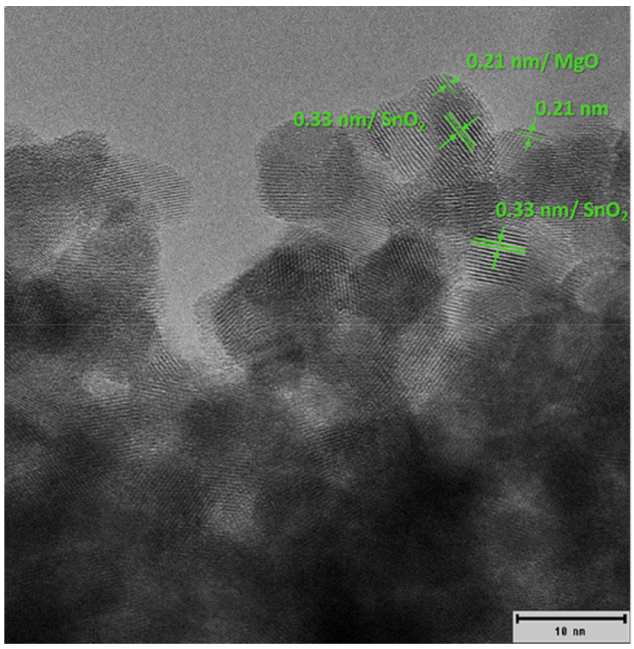

Fig. 15. TEM image of SnO_2:MgO mixture sample.

ionic diffusion in the electrolyte solution (R_d, for frequencies lower than 1 Hz) (Zainudin et al., 2019; Haddad et al., 2017; Han et al., 2006; Bisquert, 2002; Kay and Grätzel, 2002). The impedance parameters were extracted using the equivalent circuit model (inset of Fig. 16(a)), and the fitted curves are shown as solid lines in the Nyquist plots. The calculated values of the series resistance (R_S), charge-transfer resistance of the Pt/electrolyte interface (R_{Pt}), charge-transfer resistance of the SnO_2/electrolyte interface (R_{CT}) and electron diffusion resistance through photoanodes (R_d) based on the equivalent circuits for the three types of DSSCs are tabulated in Table 7.

DSSC made with bare SnO_2 photoanode shows the lowest charge transfer resistance (R_{CT}) as shown in the Table 7, i.e. the resistance against the electron recombination from SnO_2 crystals to redox electrolyte at the interface of photoanode/electrolyte. $R_{CT}$is higher for both MgO coated photoanodes. The R_{CT} values of both DSSCs made by SnO_2:MgO and Au:SnO_2:MgO have increased evidently due the presence of the thin insulating layer of MgO around the SnO_2 grains in the photoanode structure. Hence, the presence of the MgO shell in reducing recombination must have led to the enhancement of *V*OC (Tennakone et al., 2001). As shown in Table 7, the R_S, R_{Pt}, R_{CT} and R_d values of the plasmonic DSSC (Au:SnO_2:MgO) are significantly lower compared to the corresponding quantities of the reference DSSC made with SnO_2:MgO. From the R_{CT} values of DSSCs made with SnO_2:MgO and Au:SnO_2:MgO, the DSSC made with Au:SnO_2:MgO, exhibits a lower charge-transfer resistance value (24.57 Ω) indicating more efficient charge transfer processes across the SnO_2 Au NP/ electrolyte interface, while the reference DSSC made with SnO_2:MgO shows the highest value (25.89 Ω).

Moreover, the descending order of the values of R_d, the electron diffusion resistance through photoanodes, is SnO_2 > SnO_2:MgO > Au:SnO_2:MgO. When we consider the DSSCs made with SnO_2 and SnO_2:MgO photoanodes, the electron recombination rate is lower for the DSSCs made with SnO_2:MgO compared to the cells made with bare SnO_2. This means that the concentration of charge carriers in the SnO_2 network is higher for SnO_2:MgO and

the diffusion resistance is smaller compared to the pristine SnO_2.The lowest R_d value in the plasmonic DSSCs clearly shows that by incorporating Au NP into SnO_2 photoanode, the electron-transfer mechanism at the SnO_2 has been improved. The better connectivity and more conducting pathways created by the presence of metal nanoparticles within the SnO_2 nanoporous structure (photoanode) is likely to facilitate this charge transfer process, and it would be easier for the electrons released by the redox reaction at the interface to reach the dye cation across the Au: SnO_2:MgO electrode. When compared to the R_S values, the lowest resistance was observed for DSSC with bare SnO_2 photoanode than other two. As Rs represents the total series resistance of the cell, the variation of R_s value is clearly due to the different interfaces present in the DSSC structure fabricated with different photoanodes, (a) bare SnO_2, (b) FTO/SnO_2/electrolyte/Pt/FTO, (c) MgO/SnO_2, (d) FTO/MgO:SnO_2/electrolyte/Pt/FTO and (e) Plasmonic photoanode, FTO/ Au:MgO:SnO_2/

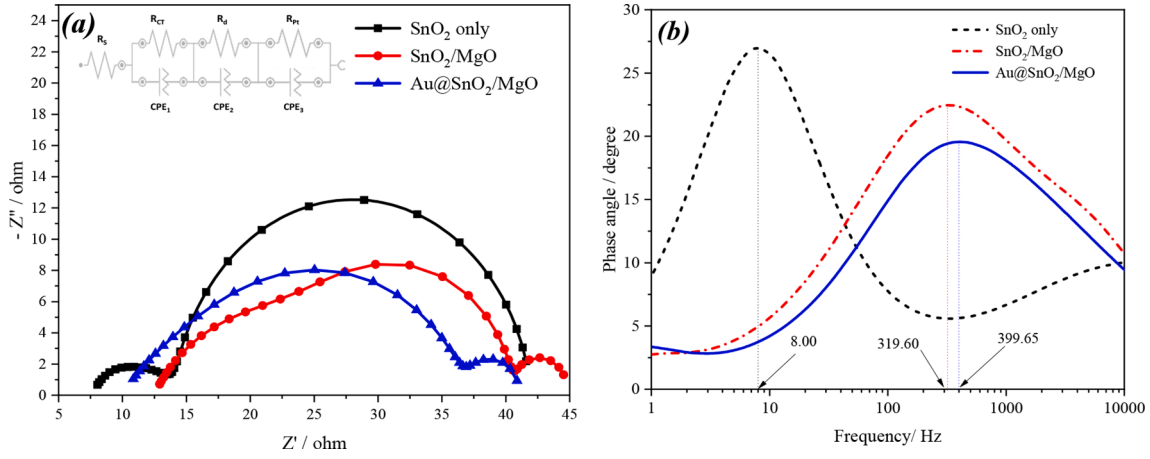

Fig. 16. (a) Impedance Nyquist plots and (b) Bode phase plots for three different DSSCs made with bare SnO_2, SnO_2:MgO and Au:SnO_2:MgO photoanodes.

Table 7
Interfacial photoelctrochemical resistances and electron life time obtained from EIS measurements of DSSCs made from three different SnO_2-based photoanodes.

Photoanode	V_{OC} (mV)	J_{SC} (mA cm^{-2})	Efficiency (%)	R_S	R_{Pt}	R_{CT}	R_d	f_{max} (Hz)	τ_e (ms)
SnO_2	452.2	6.07	1.52	7.55	8.76	19.78	6.2	8.00	19.9
SnO_2:MgO	715.8	7.98	4.19	12.5	12.43	25.89	4.06	319.60	0.5
Au: SnO_2:MgO	725.6	9.06	4.69	9.98	10.29	24.57	3.89	399.65	0.4

electrolyte/Pt/FTO. When we introduce the MgO insulating layer, R_s values of SnO2:MgO and Au:SnO2:MgO are higher than bare SnO_2. Due to creating more pathways and better connectivity by the presence of metal Au nanoparticles has reduced the series resistance of Au:SnO_2:MgO than SnO_2:MgO.

From the bode phase plots of EIS spectra (Fig. 16(b)), the effective electron lifetime (τ_e) can be estimated from the maximum frequency (f_{max}) at the peak of the intermediate impedance semicircle at middle frequencies as in the following equation (Sewvandi et al., 2014);

$$\tau_e = \frac{1}{\omega_{max}} = \frac{1}{2\pi f_{max}}$$

As shown in the Fig. 16 (b), the value of f_{max} of both SnO_2:MgO O and Au: SnO_2:MgO photoanodes has shifted towards the higher frequency side. The effective electron lifetimes (τ_e) for these DSSCs calculated by using the above equations are tabulated in Table 7. According to these values, the electron life time was highest for the reference cell (with pristine SnO_2) and J_{SC} of this cell was the lowest. τ_e values of other two cells (SnO_2:MgO and Au: SnO_2:MgO) were significantly lower and their J_{SC} values were higher compared to the reference cell. As the impedance measurements were taken under the exposed light condition, shorter life time at the photoanode means faster charge transfer, easy charge diffusion and lower recombination. Therefore, the Au: SnO_2:MgO photoanode has promoted the charge transfer and increased the rate of electrons arriving at the collecting counter electrode. This has led to the enhancement in $J_{SC}$and the efficiency of the plasmonic solar cells.

4. Conclusion

The enhancement in photovoltaic performance in DSSCs made with SnO_2 photoanode by introducing a MgO insulating layer has been further strengthened by making use of the local surface plasmon resonance effect by Au nanoparticles incorporated in SnO_2:MgO photoanode. It was observed that the efficiency enhancement of these plasmonic DSSCs for a selected size range of Au nanoparticles depends strongly on the added amount of AuNPs and showed a maximum for the optimized amount of AuNPs incorporated into the SnO_2:MgO photoanode. Compared with the normal DSSC made with pristine SnO_2 photoanode, the short-circuit current density (J_{SC}), open-circuit voltage (V_{OC}) and the fill factor (FF) of the DSSCs made with SnO_2:MgO and Au NP-incorporated Au:SnO_2:MgO photoanodes exhibited an enhancement in the overall solar cell efficiency by ~175% for the SnO_2:MgO based DSSC and ~208% for the plasmonic DSSC with Au: SnO_2:MgO based DSSC. Based on consistent results from several different types of electrochemical and optical measurements, it can be established that the AuNP incorporated plasmonic DSSCs exhibit a high optical absorption characterized by the red shift in the IPCE peak maximum and a significantly-enhanced optical absorption induced by the surface plasmon resonance effect, enhancing the short-circuit current density, J_{sc} and the efficiency. These findings are also supported by reduced electron life times of the DSSC made with Au: SnO_2:MgO composite photoanode.

Declaration of Competing Interest

The authors declare that they have no known competing financial interests or personal relationships that could have appeared to influence the work reported in this paper.

Acknowledgement

Authors wish to acknowledge the assistance provided by Mr. Y.M.I.B. Samarakoon for XRD measurements.

References

Birkel, A., Lee, Y.-G., Koll, D., Meerbeek, X.V., Frank, S., Choi, M.J., Kang, Y.S., Char, K., Tremel, W., 2012. Highly efficient and stable dye-sensitized solar cells based on SnO 2 nanocrystals prepared by microwave-assisted synthesis. Energy Environ. Sci. 5 (1), 5392–5400.

O'Regan, B., Grätzel, M., 1991. A low-cost, high-efficiency solar cell based on dye-sensitized colloidal TiO2 films. Nature. 353 (6346), 737–740. https://doi.org/10.1038/353737a0.

Gong, J., Sumathy, K., Qiao, Q., Zhou, Z., 2017. Review on dye-sensitized solar cells (DSSCs): Advanced techniques and research trends. Renew. Sustain. Energy Rev. 68, 234–246. https://doi.org/10.1016/j.rser.2016.09.097.

Snaith, H.J., Ducati, C., 2010. SnO_2-Based dye-sensitized hybrid solar cells exhibiting near unity absorbed photon-to-electron conversion efficiency. Nano Lett. 10 (4), 1259–1265. https://doi.org/10.1021/nl903809r.

Baraneedharan, P., Chidambaram, S., Kasi, N., Muthusamy, S., 2014. Recent advances in SnO2 based photo anode materials for third generation photovoltaics. in 25–38.

Bhande, S.S., Shinde, D.V., Tehare, K.K., Patil, S.A., Mane, R.S., Naushad, M., Alothman, Z.A., Hui, K.N., Han, S.H., 2014. DSSCs synergic effect in thin metal oxide layer-functionalized SnO2 photoanodes. J. Photochem. Photobiol. A Chem. 295, 64–69. https://doi.org/10.1016/j.jphotochem.2014.09.004.

Zainudin, S.N.F., Abdullah, H., Markom, M., 2019. Electrochemical studies of tin oxide based-dye-sensitized solar cells (DSSC): a review. J. Mater. Sci. Mater. Electron. 30 (6), 5342–5356. https://doi.org/10.1007/s10854-019-00929-6.

Wali, Q., Bakr, Z.H., Manshor, N.A., Fakharuddin, A., Jose, R., 2016. SnO2-TiO2 hybrid nanofibers for efficient dye-sensitized solar cells. Sol. Energy. 132, 395–404. https://doi.org/10.1016/j.solener.2016.03.037.

Tennakone, K., Bandara, J., Bandaranayake, P.K.M., Kumara, G.R.A., Konno, A., 2001. Enhanced Efficiency of a Dye-Sensitized Solar Cell Made from MgO-Coated Nanocrystalline SnO2. Jpn. J. Appl. Phys. 40, L732–L734. https://doi.org/10.1143/jjap.40.l732.

Senadeera, G.K.R., Weerasinghe, A.M.J.S., Dissanayake, M.A.K.L., Thotawatthage, C.A., 2018. A five-fold efficiency enhancement in dye sensitized solar cells fabricated with AlCl3 treated, SnO2 nanoparticle/nanofibre/nanoparticle triple layered photoanode. J. Appl. Electrochem. 48 (11), 1255–1264. https://doi.org/10.1007/s10800-018-1247-6.

Sato, N., 1998. Electrochemistry at Metal and Semiconductor Electrodes, 1st ed. Elsevier Science.

Augusto, A., Herasimenka, S.Y., King, R.R., Bowden, S.G., Honsberg, C., 2017. Analysis of the recombination mechanisms of a silicon solar cell with low bandgap-voltage offset. J. Appl. Phys. 121. http://aip.scitation.org/doi/10.1063/1.4984071http://aip.scitation.org/doi/pdf/10.1063/1.4984071http://aip.scitation.org/doi/pdf/10.1063/1.4984071http://aip.scitation.org/doi/am-pdf/10.1063/1.4984071.

Sinton, R.A., Cuevas, A., 1996. Contactless determination of current-voltage characteristics and minority-carrier lifetimes in semiconductors from quasi-steady-state photoconductance data. Appl. Phys. Lett. 69 (17), 2510–2512. https://doi.org/10.1063/1.117723.

Meen, T.-H., Tsai, J.-K., Chao, S.-M., Lin, Y.-C., Wu, T.-C., Chang, T.-Y., Ji, L.-W., Water, W., Chen, W.-R., Tang, I.-T., Huang, C.-J., 2013. Surface plasma resonant effect of gold nanoparticles on the photoelectrodes of dye-sensitized solar cells. Nanoscale Res. Lett. 8, 450. https://doi.org/10.1186/1556-276X-8-450.

Chandrasekharan, N., Kamat, P.V., 2000. Improving the Photoelectrochemical Performance of Nanostructured TiO 2 Films by Adsorption of Gold Nanoparticles †. J. Phys. Chem. B - J PHYS CHEM B. 104 (46), 10851–10857. https://doi.org/10.1021/jp0010029.

Dissanayake, M.A.K.L., Jaseetharan, T., Senadeera, G.K.R., Kumari, J.M.K.W., 2020. Efficiency enhancement in PbS/CdS quantum dot-sensitized solar cells by plasmonic Ag nanoparticles. J. Solid State Electrochem. 24 (2), 283–292. https://doi.org/10.1007/s10008-019-04420-4.

Aponsu, G., De Silva, R., Perera, V., 2010. Enhanced photovoltaic effects of dye-sensitized solar cells of SnO_2 surface modified with gold nano particles. Sri Lankan J. Phys. 9, 27. https://doi.org/10.4038/sljp.v9i0.2508.

Dissanayake, M.A.K.L., Kumari, J.M.K.W., Senadeera, G.K.R., Thotawatthage, C.A., 2016. Efficiency enhancement in plasmonic dye-sensitized solar cells with TiO2 photoanodes incorporating gold and silver nanoparticles. J. Appl. Electrochem. 46 (1), 47–58. https://doi.org/10.1007/s10800-015-0886-0.

Notarianni, M., Vernon, K., Chou, A., Aljada, M., Liu, J., Motta, N., 2014. Plasmonic effect of gold nanoparticles in organic solar cells. Sol. Energy. 106, 23–37. https://doi.org/10.1016/j.solener.2013.09.026.

Mandal, P., Sharma, S., 2016. Progress in plasmonic solar cell efficiency improvement: A status review. Renew. Sustain. Energy Rev. 65, 537–552. https://doi.org/10.1016/j.rser.2016.07.031.

Amir Tabrizi, H.A., Ayhan, F., Introduction, H., 2009. J. Biol. Chem. 37, 217–226. http://www.hjbc.hacettepe.edu.tr/site/assets/files/2941/37_3_217-226.pdf.

Huang, H., Yang, X., 2003. Chitosan mediated assembly of gold nanoparticles multilayer. Colloids Surfaces A Physicochem. Eng. Asp. 226 (1-3), 77–86. https://doi.org/10.1016/S0927-7757(03)00382-0.

Kumari, J.M.K.W., Senadeera, G.K.R., Dissanayake, M.A.K.L., Thotawatthage, C.A., 2017. Dependence of photovoltaic parameters on the size of cations adsorbed by TiO2 photoanode in dye-sensitized solar cells. Ionics (Kiel). 23 (10), 2895–2900. https://doi.org/10.1007/s11581-017-1995-z.

Njoki, P.N., Lim, I.-I., Mott, D., Park, H.-Y., Khan, B., Mishra, S., Sujakumar, R., Luo, J., Zhong, C.-J., 2007. Size correlation of optical and spectroscopic properties for gold nanoparticles. J. Phys. Chem. C. 111 (40), 14664–14669. https://doi.org/10.1021/jp074902z.

Hägglund, C., Zäch, M., Kasemo, B., 2008. Enhanced charge carrier generation in dye sensitized solar cells by nanoparticle plasmons. Appl. Phys. Lett. 92 (1), 013113. https://doi.org/10.1063/1.2830817.

Kumari, J.M.K.W., Sanjeevadharshini, N., Dissanayake, M.A.K.L., Senadeera, G.K.R., Thotawatthage, C.A., 2016. The effect of TiO2 photo anode film thickness on photovoltaic properties of dye-sensitized solar cells. Ceylon J. Sci. 45, 33–41. https://doi.org/10.4038/cjs.v45i1.7362.

Rand, B.P., Peumans, P., Forrest, S.R., 2004. Long-range absorption enhancement in organic tandem thin-film solar cells containing silver nanoclusters. J. Appl. Phys. 96 (12), 7519–7526. https://doi.org/10.1063/1.1812589.

K. Umair, M.A.K.L. Dissanayake, G.K.R. Senadeera, Efficiency enhancement in SnO_2 based dye-sensitized solar cells by incorporating plasmonic gold nanoparticles, in: PGIS Res. Congr. 2020 Proc., Postgraduate Institute of Science (PGIS), University of Peradeniya, Peradeniya, Sri Lanka, 2020: p. 214. http://www.pgis.pdn.ac.lk/rescon2020/doc/rescon2020_proceedings.pdf.

Hagfeldt, A., Lindquist, S., Gratzel, M., 1994. Charge carrier separation and charge transport in nanocrystalline junctions. Sol. Energy Mater. Sol. Cells. 32 (3), 245–257. https://doi.org/10.1016/0927-0248(94)90262-3.

Ramakrishna, G., Das, A., Ghosh, H.N., 2004. Effect of Surface Modification on Back Electron Transfer Dynamics of Dibromo Fluorescein Sensitized TiO2 Nanoparticles. Langmuir. 20 (4), 1430–1435. https://doi.org/10.1021/la035190g10.1021/la035190g.s001.

Patel, M., Zafaryab, M., Rizvi, M., Agrawal, V., Ansari, Z., Malhotra, B., Ansari, S.G., 2013. Antibacterial and Cytotoxic Effect of Magnesium Oxide Nanoparticles on Bacterial and Human Cells. Journal of Nanoengineering and Nanomanufacturing. 3, 162–166. https://doi.org/10.1166/jnan.2013.1122.

Haddad, N., Ayadi, Z., Mahdhi, H., Djessas, K., 2017. Influence of fluorine doping on the microstructure, optical and electrical properties of SnO2 nanoparticles. Journal of Materials Science: Materials in Electronics. 28 https://doi.org/10.1007/s10854-017-7433-1.32].

Han, L., Koide, N., Chiba, Y., Islam, A., Mitate, T., 2006. Modeling of an equivalent circuit for dye-sensitized solar cells: improvement of efficiency of dye-sensitized solar cells by reducing internal resistance. Comptes Rendus Chim. 9 (5-6), 645–651. https://doi.org/10.1016/j.crci.2005.02.046.

Sewvandi, G.A., Tao, Z., Kusunose, T., Tanaka, Y., Nakanishi, S., Feng, Q.i., 2014. Modification of TiO2 Electrode with Organic Silane Interposed Layer for High-Performance of Dye-Sensitized Solar Cells. ACS Appl. Mater. Interfaces. 6 (8), 5818–5826. https://doi.org/10.1021/am500666e.

Bisquert, J., 2002. Analysis of the kinetics of ion intercalation: Ion trapping approach to solid-state relaxation processes. Electrochim. Acta. 47 (15), 2435–2449. https://doi.org/10.1016/S0013-4686(02)00102-0.

Kay, A., Grätzel, M., 2002. Dye-Sensitized Core−Shell Nanocrystals: Improved Efficiency of Mesoporous Tin Oxide Electrodes Coated with a Thin Layer of an Insulating Oxide. Chem. Mater. 14 (7), 2930–2935. https://doi.org/10.1021/cm0115968.